Ab initio calculations on low-lying electronic states of SbO_2^- and Franck-Condon simulation of its photodetachment spectrum

Edmond P. F. Lee[a)]
Department of Applied Biology and Chemical Technology, The Hong Kong Polytechnic University, Hung Hom, Hong Kong

John M. Dyke
School of Chemistry, University of Southampton, Highfield, Southampton SO17 1BJ, United Kingdom

Daniel K. W. Mok[b),c)] and Foo-tim Chau[b),d)]
Department of Applied Biology and Chemical Technology, The Hong Kong Polytechnic University, Hung Hom, Hong Kong

Wan-ki Chow
Department of Building Services Engineering, The Hong Kong Polytechnic University, Hung Hom, Hong Kong

(Received 14 November 2006; accepted 10 July 2007; published online 6 September 2007)

Geometry optimization and harmonic vibrational frequency calculations have been carried out on the low-lying singlet and triplet electronic states of the antimony dioxide anion (SbO_2^-) employing a variety of *ab initio* methods. Both large-core and small-core relativistic effective core potentials were used for Sb in these calculations, together with valence basis sets of up to augmented correlation-consistent polarized-valence quintuple-zeta (aug-cc-pV5Z) quality. The ground electronic state of SbO_2^- is determined to be the $\tilde{X}\,^1A_1$ state, with the $\tilde{a}\,^3B_1$ state, calculated to be ~48 kcal mole^{-1} (2.1 eV) higher in energy. Further calculations were performed on the $\tilde{X}\,^2A_1$, $\tilde{A}\,^2B_2$, and $\tilde{B}\,^2A_2$ states of SbO_2 with the aim to simulating the photodetachment spectrum of SbO_2^-. Potential energy functions (PEFs) of the $\tilde{X}\,^1A_1$ state of SbO_2^- and the $\tilde{X}\,^2A_1$, $\tilde{A}\,^2B_2$, and $\tilde{B}\,^2A_2$ states of SbO_2 were computed at the complete-active-space self-consistent-field multireference internally contracted configuration interaction level with basis sets of augmented correlation-consistent polarized valence quadruple-zeta quality. Anharmonic vibrational wave functions obtained from these PEFs were used to compute Franck-Condon factors between the $\tilde{X}\,^1A_1$ state of SbO_2^- and the $\tilde{X}\,^2A_1$, $\tilde{A}\,^2B_2$, and $\tilde{B}\,^2A_2$ states of SbO_2, which were then used to simulate the photodetachment spectrum of SbO_2^-, which is yet to be recorded experimentally. © *2007 American Institute of Physics*. [DOI: 10.1063/1.2768355]

INTRODUCTION

Sb and Bi clusters are very interesting species showing a semimetal to semiconductor transition. This is very important for thermoelectronic nanodevices, such as with one-dimensional nanostructured materials including nanowires, nanorods, nanobelts, and nanotubes, which have applications as interconnect and functional units in electronic, optoelectronic, electrochemical, thermoelectric, and electromechanical nanodevices (see for example, Refs. 1 and 2, and references therein). Since these clusters can be easily oxidized, studies of their oxides, as well as their oxide anions, are very important. In addition, antimony oxide has very important catalytic applications, such as in the direct synthesis of acrylonitrile from propane rather than from propene[3] and in the extremely demanding catalytic partial oxidation of methane to methanol[4] (see also Refs. 5 and 6, and references therein). In these connections, we have recently reported two *ab initio* studies on antimony dioxide (SbO_2) and its cation (SbO_2^+).[5,6] In these studies, the ground electronic states of SbO_2 and SbO_2^+ have been established to be the $\tilde{X}\,^2A_1$ and $\tilde{X}\,^1A_1$ states, respectively. In addition, some low-lying doublet and quartet excited states of SbO_2,[5,6] and low-lying singlet and triplet excited states of SbO_2^+,[5] were investigated. Reliable adiabatic and/or vertical excitation and ionization energies from the $\tilde{X}\,^2A_1$ state of SbO_2 to low-lying excited states of SbO_2 and states of SbO_2^+, respectively, were computed with a view to assist future spectroscopic identification of SbO_2 and SbO_2^+ via their electronic spectra, using methods such as absorption or laser induced fluorescence spectroscopy and/or ultraviolet photoelectron spectroscopy, which are yet to be recorded. Completing this series of computational studies on antimony dioxide and its ions, we report *ab initio* calculations on low-lying singlet and triplet states of the anion of antimony dioxide (SbO_2^-). Additional *ab initio* calculations have been

[a)]Also at Department of Building Services Engineering, The Hong Kong Polytechnic University and School of Chemistry, University of Southampton. Electronic mail: epl@soton.ac.uk
[b)]Authors to whom correspondence should be addressed.
[c)]Electronic mail: bcdaniel@polyu.edu.hk
[d)]Electronic mail: bcftchau@polyu.edu.hk

TABLE I. Basis sets used for Sb.

Basis	ECP[a]	Valence set[a]	Augmented[b]	Frozen[c]	Correlated[d]	Nb[e]
A	ECP28MDF	Aug-cc-pVTZ		$4s4p4d$	$5s^25p^3$	147
B	ECP46MWB	Aug-cc-pVQZ			$5s^25p^3$	239
B1	ECP46MWB	Aug-cc-pVQZ($spdf$)[f]			$5s^25p^3$	185
B2	ECP46MWB	d-aug-cc-pVQZ[g]			$5s^25p^3$	314
B_SO	ECP46MDF[h]	Uncontracted spd[h]			$5s^25p^3$	176
DZVP		Uncontracted spd[i]				163
C	ECP28MDF	Aug-cc-pV5Z		$4s4p4d$	$5s^25p^3$	393
D	ECP28MDF	Aug-cc-pV5Z	$3d2f2g2h$	$4s4p$	$4d^{10}5s^25p^3$	462
E	ECP28MDF	Aug-cc-pV5Z	$3s3p3d3f2g2h$		$4s^24p^64d^{10}5s^25p^3$	481

[a]Standard effective core potentials and valence basis sets for Sb are published. The ECP46MWB_aug-cc-pVQZ and ECP28MDF_aug-cc-pV5Z basis sets are from the MOLPRO basis set library. The ECP46MWB_aug-cc-pVQZ basis set is the same as the SDB-aug-cc-pVQZ basis from Ref. 8. The ECP28MDF_aug-cc-pVXZ (X=T and 5) basis sets are the same as aug-cc-pVXZ-PP (X=T and 5) basis sets, respectively, from the EMSL basis set library (Ref. 10). For the ECP46MWB and ECP28MDF ECPs, see http://www.theochem.uni-stuttgart.de/cgi-bin/pe.sh?References and Ref. 9. The corresponding aug-cc-pVXZ (X=T, Q, and 5) basis sets were used for O and the O $1s^2$ electrons are frozen in all the correlation calculations.
[b]See Ref. 6 for details of these augmented basis functions designed for Sb.
[c]Although these shells of Sb are accounted for by the basis sets used, they are frozen in the correlation calculations. The O $1s^2$ electrons are frozen in all correlation calculations.
[d]These Sb electrons are correlated. The O $2s^22p^4$ electrons are correlated in all correlation calculations [i.e., these electrons are correlated in the RCCSD(T) calculations and are active in CASSCF/MRCI calculations; the CASSCF/MRCI calculations have a full valence active space and included all these electrons].
[e]Total numbers of contracted Gaussian functions in the basis sets for SbO_2.
[f]Only s, p, d, and f functions (i.e., no g functions).
[g]Double-augmented quality basis sets: d-aug-cc-pVQZ for O and ECP46MWB_aug-cc-pVQZ plus a second diffuse set of s(0.009 980), p(0.006 644 52), d(0.019 238 27), f(0.036 892 6), and g(0.082 861 3) functions for Sb.
[h]In CASSCF spin-orbit interaction calculations using the spin-orbit effective core potential, ECP46MDF (see http://www.theochem.uni-stuttgart.de/pseudopotentials/clickpse.en.html), the uncontracted s, p, and d functions from the ECP46MWB_aug-cc-pVQZ basis set of Sb (coupled with uncontracted s, p, and d functions from the aug-cc-pVQZ basis and of O) were employed (see text).
[i]Uncontracted s, p, and d functions of the DZVP-DFT-orb basis sets for Sb and O were employed in CASSCF spin-orbit interaction calculations using the Breit-Pauli operator (see text).

carried out on SbO_2 in order to simulate the photodetachment spectrum of SbO_2^-. To our knowledge, no previous experimental or computational study has been carried out on SbO_2^-. It is noted, however, that the photodetachment spectrum of PO_2^- was reported ten years ago.[7]

THEORETICAL CONSIDERATIONS AND COMPUTATIONAL DETAIL

Ab initio calculations

The basis sets used in the present study, including large-core and small-core effective core potentials (ECPs) employed for Sb, associated valence basis functions,[8–10] augmented tight functions[6] to the small-core ECP basis set, ECP28MDF_aug-cc-pV5Z for outer core electrons of Sb, and other details, such as the corresponding frozen core used and electrons to be correlated in the correlation calculations, are summarized in Table I (see Ref. 6 for more information on the basis sets used). The computational strategy of the present study essentially follows that of our previous work[5,6] and hence will not be repeated here. Briefly, initial survey calculations were carried out at relatively low levels of theory (e.g., CASSCF, MP2, B3LYP, HCTH407, and PW91PW91) with relatively small basis sets (e.g., basis sets A and B1; see Table I). Further higher level calculations [e.g., CASSCF/MRCI and RCCSD(T)] with larger basis sets (e.g., basis sets C, D, and E; see Table I) were then performed in order to obtain more reliable minimum-energy geometries, harmonic vibrational frequencies, and relative electronic energies.

Spin-orbit (SO) interaction calculations were carried out between low-lying states of SbO_2 as described previously[5,6] using either the Breit-Pauli operator or a SO pseudopotential and averaged-state CASSCF wave functions of the states involved. These calculations are for the purpose of assessing the effects of SO coupling on computed relative electronic energies, such as vertical photodetachment energies (VDEs). Although all electronic states considered in the present study are nondegenerate states (all states of C_{2v} symmetry are nondegenerate states) and hence there is no first order or diagonal spin-orbit interaction in these states, off-diagonal spin-orbit interactions between states, which are close to each other in energy, may be significant for a molecule containing the heavy fourth row element Sb. When the Breit-Pauli operator was employed, uncontracted s, p, and d functions of the all-electron DZVP-DFT-orb basis sets[11] were used for Sb and O. When the SO pseudopotential of the ECP46MDF ECP (Ref. 12) was used in the SO interaction calculations, uncontracted s, p, and d functions of the ECP46MWB_aug-cc-pVQZ and aug-cc-pVQZ basis sets were used for Sb and O, respectively. (The ECP basis set used for Sb in these SO calculations is denoted as B_SO in Table I.) The computed contributions of SO coupling to the electronic energies of the $\tilde{X}\,^2A_1$, $\tilde{A}\,^2B_2$, and $\tilde{B}\,^2A_2$ states of SbO_2 are −2.9, +0.6, and +2.3 (−2.2, −11.0, and +13.1) cm^{-1}, with the Breit-Pauli operator (SO pseudopotential), respectively, at the RCCSD(T)/D geometry of the $\tilde{X}\,^1A_1$ state of SbO_2^- using the RCCSD(T)/D electronic energies for the diagonal SO matrix elements. These SO contributions of smaller than 0.002 eV suggest that SO effects on the computed relative electronic

TABLE II. The ranges of bond lengths [r(SbO) in Å] and bond angles [θ(OSbO) in deg], the number of points of the CASSCF/MRCI/ECP46MWB_aug-cc-pVQZ, aug-cc-pVQZ (for Sb, O, respectively) energy scans, which were used for the fitting of the potential energy functions (PEFs) of the $\tilde{X}\,^1A_1$ state of SbO_2^- and the $\tilde{X}\,^2A_1$, $\tilde{A}\,^2B_2$, and $\tilde{B}\,^2A_2$ states of SbO_2, and the maximum vibrational quantum numbers of the symmetric stretching (v_1) and bending (v_2) modes of the harmonic basis used in the variational calculations of the anharmonic vibrational wave functions of each electronic state and the restrictions of the maximum values of (v_1+v_2).

States	Range of r	Range of θ	Points	Max. v_1	Max. v_2	Max. (v_1+v_2)
$\tilde{X}\,^1A_1$	1.2–2.37	65–168	125	6	20	20
$\tilde{X}\,^2A_1$	1.52–2.35	78–168	94	5	12	15
$\tilde{A}\,^2B_2$	1.3–2.25	52–151	119	8	26	26
$\tilde{B}\,^2A_2$	1.17–2.47	56–166	117	6	20	20

energies of these low-lying states of SbO_2 are negligibly small in the Franck-Condon region of the photodetachment spectrum of SbO_2^-. In addition, as will be discussed in the next section, the lowest excited state of SbO_2^-, the $\tilde{a}\,^3B_1$ state, has been calculated to be considerably higher in energy than the $\tilde{X}\,^1A_1$ state [>48 kcal mole^{-1} (2.0 eV); see the next section]. Consequently, off-diagonal SO interaction between the $\tilde{X}\,^1A_1$ state and low-lying excited states of SbO_2^- is expected to be negligibly small. In view of the above considerations, SO effects have been ignored in the calculations of the potential energy surfaces discussed below.

For the fitting of the potential energy functions (PEFs), complete-active-space self-consistent field (CASSCF)/multireference configuration interaction (plus the Davidson correction) energies of the $\tilde{X}\,^1A_1$ state of SbO_2^- and the $\tilde{X}\,^2A_1$, $\tilde{A}\,^2B_2$, and $\tilde{B}\,^2A_2$ states of SbO_2 were calculated employing basis set B. The multireference CASSCF/MRCI method was employed in these energy scans because in some regions of the potential energy surfaces of the electronic states considered, which are far away from the respective equilibrium geometries, multireference character was found to be significant. The ranges of the geometrical parameters and the total number of energy points for each state covered by the energy scans are given in Table II. These energy points have excluded those whose largest CI coefficients in the MRCI wave function have computed values of less than 0.70. In addition, all the energy points included in the ranges given in Table II and used for the fitting of the PEFs have computed values of the sum of the squares of the CI coefficients of all reference configurations $\Sigma(C_{\mathrm{ref}})^2$ larger than 0.93, indicating that the MRCI wave functions are adequate for the states in the regions concerned. All calculations of the present study were performed using the MOLPRO suite of programs.[13]

Potential energy functions, anharmonic vibrational wave functions, and Franck-Condon factor calculations

For each electronic state studied, the PEF, V, was determined by fitting the following polynomial to an appropriate number of single point energies as discussed above:

$$V=\sum_{ij} C_{ij}(S_1)^i(S_2)^j + V_{\mathrm{eqm}}. \tag{1}$$

In this equation, S_1 (the symmetric stretching coordinate) is expressed in terms of a Morse type coordinate,[14]

$$S_1=[1-e^{-\gamma(r-r_{\mathrm{eqm}})/r_{\mathrm{eqm}}}]/\gamma, \tag{2}$$

where r is the SbO bond length and r_{eqm} is the equilibrium bond length. S_2 (the symmetric bending coordinate) is expressed as

$$S_2=\Delta\theta+\alpha\Delta\theta^2+\beta\Delta\theta^3, \tag{3}$$

where $\Delta\theta$ is the displacement in the θ(OSbO) bond angle from the corresponding equilibrium value.[15] The nonlinear least squares fitting procedure,[16] NL2SOL, was employed to obtain the C_{ij}'s, V_{eqm}, r_{eqm}, θ_{eqm}, α, β, and γ values from the computed single point energy data. The asymmetric stretching mode has not been considered because for the photodetachment of an electron from a C_{2V} anion to a C_{2V} neutral molecule, this mode is only allowed in double quantum excitations.

Variational calculations, which employed the rovibrational Hamiltonian of Watson for a nonlinear molecule[17] and the *ab initio* PEFs discussed above, were carried out to obtain the anharmonic vibrational wave functions and their corresponding energies (see Refs. 18 and 19 for details). The anharmonic vibrational wave functions were expressed as linear combinations of harmonic oscillator functions $h(v_1,v_2)$, where v_1 and v_2 denote the quantum numbers of the harmonic basis functions for the symmetric stretching and bending modes, respectively.[18,20] The maximum v_1 and v_2 values of the harmonic basis used and the restriction of the maximum value of (v_1+v_2) imposed for each electronic state studied are given in Table II. Franck-Condon (FC) factors were computed employing anharmonic vibrational wave functions and allowing for the Duschinsky rotation, as described previously.[18,20]

Three photodetachment bands of SbO_2^-, which lead to the $\tilde{X}\,^2A_1$, $\tilde{A}\,^2B_2$, and $\tilde{B}\,^2A_2$ states of SbO_2 via one-electron allowed photodetachment processes from the $\tilde{X}\,^1A_1$ state of SbO_2^-, have been simulated. From our previous study[6] on the low-lying electronic states of SbO_2, the fourth one-electron allowed photodetachment band of SbO_2^- should be to the $\tilde{C}\,^2B_1$ state of SbO_2, with an electron affinity (EA) of over 4.7 eV, estimated from a computed T_e value of 1.158 eV at

TABLE III. Computed vertical excitation energies [from the $\tilde{X}\,^1A_1$ state [at the CCSD(T)/B optimized geometry of the $\tilde{X}\,^1A_1$ state]; T_v in kcal/mole], major electronic configurations, and the corresponding computed CI coefficients in the MRCI wave functions (C_{ref}) of some low-lying singlet and triplet states of SbO_2^- obtained from CASSCF/MRCI/B calculations (see text).

States	Configurations	C_{ref}	T_v(CAS)	T_v(MRCI)	T_v(MRCI+D)
$^1A_1$	$(5a_1)^2(1b_1)^2(4b_2)^2(1a_2)^2$	0.895	0	0	0
	$(5a_1)^2(2b_1)^2(4b_2)^2(1a_2)^0$	−0.125			
$^3B_1$	$(5a_1)^1(2b_1)^1(4b_2)^2(1a_2)^2$	0.892	53.2	51.9	50.9
	$(5a_1)^2(2b_1)^2(4b_1)^1(1a_2)^1$	0.138			
$^1B_1$	$(5a_1)^1(2b_1)^1(4b_2)^2(1a_2)^2$	0.880	62.6	62.4	61.6
	$(5a_1)^2(2b_1)^2(4b_2)^1(1a_2)^1$	0.188			
$^3B_2$	$(5a_1)^2(2b_1)^1(4b_2)^2(1a_2)^1$	0.905	59.2	63.1	63.2
	$(5a_1)^1(1b_1)^1(2b_1)^1(4b_2)^1(1a_2)^2$	0.119			
$^3A_2$	$(5a_1)^2(2b_1)^1(4b_2)^1(1a_2)^2$	0.884	63.9	64.9	64.5
	$(5a_1)^1(2b_1)^2(4b_2)^2(1a_2)^1$	−0.171			
$^1A_2$	$(5a_1)^2(2b_1)^1(4b_2)^1(1a_2)^2$	0.880	65.6	67.0	66.9
	$(5a_1)^1(2b_1)^2(4b_2)^2(1a_2)^1$	0.190			
$^1B_2$	$(5a_1)^2(2b_1)^1(4b_2)^2(1a_2)^1$	0.858	89.0	86.1	84.5
	$(5a_1)^1(1b_1)^1(2b_1)^1(4b_2)^1(1a_2)^2$	−0.170			
$^3A_1$	$(5a_1)^2(1b_1)^1(2b_1)^1(4b_2)^2(1a_2)^2$	0.877	98.7	95.7	94.0
	$(6a_1)^1(2b_1)^1(4b_2)^1(1a_2)^1$	−0.204			

the RCCSD(T)/B level of calculation. Assuming that the fourth harmonic of a Q-switched Nd^{3+} doped yttrium aluminum garnet laser, which has a photon energy of 266 nm (4.66 eV), is used as the photon source in the photodetachment experiment (see, for example, Refs. 21 and 22), only the first three photodetachment bands of SbO_2^- are expected to be observed. The relative intensity of each vibrational component in a simulated photodetachment band is given by the corresponding computed anharmonic FC factor. Each photodetachment band was simulated assuming a Boltzmann distribution population of the low-lying vibrational levels of the $\tilde{X}\,^1A_1$ state of SbO_2^- at a vibrational temperature of 300 K.

RESULTS AND DISCUSSION

Ab initio calculations

Some of the representative and/or higher level *ab initio* results obtained are summarized in Tables III–VI. Firstly, the computed relative electronic energies (vertical excitation energies T_v from the $\tilde{X}\,^1A_1$ state of SbO_2^-) of eight low-lying electronic states of SbO_2^- obtained at the CASSCF/MRCI/B level of calculation and also the two electronic configurations with the largest computed CI coefficients in the MRCI wave function of each state are given in Table III. In all cases, the largest CI coefficient of each state is larger than 0.85, indicating that CI mixing is in general small for all these states in the vertical excitation region (from the $\tilde{X}\,^1A_1$ state of SbO_2^-). Therefore, it is concluded that single reference correlation methods should be adequate for these low-lying anionic states of SbO_2^-. Table IV gives the minimum-energy geometries and the computed relative electronic energies of some of the lowest-lying electronic states of $SbO_2^-(T_e)$ obtained at different levels of calculation.

From Tables III and IV, the following conclusions can be made. First, the ground electronic state of SbO_2^- is unambiguously the $\tilde{X}\,^1A_1$ state, as all the excited states considered are significantly higher in energy (over 2.0 eV or ~50 kcal mole^{-1}) both adiabatically (Table IV) and vertically (Table III). Second, the lowest excited state is the $\tilde{a}\,^3B_1$ state, which was calculated to be ~48 kcal mole^{-1} higher in energy than the $\tilde{X}\,^1A_1$ state (i.e., T_e=2.0 eV) at the highest level of calculation. Third, calculations at lower levels, such as with the CASSCF, MP2, or density functional theory (DFT) methods (with the different functionals shown in Table IV), appear to be unreliable regarding the order of the low-lying excited states and/or computed relative electronic energies. For example, the $^3B_2$ state was computed to be slightly lower in energy than the $^3B_1$ state at the CASSCF/B1 level of calculation, contrary to RCCSD(T) results, which have the $^3B_2$ state higher in energy than the $^3B_1$ state by ~8 kcal mole^{-1} (0.35 eV) with the two basis sets, B and C, used (Table IV). Also, the computed T_e values of the $\tilde{a}\,^3B_1$ state of ~41 kcal mole^{-1} obtained from DFT calculations are smaller than those obtained from RCCSD(T) calculations by at least 7 kcal mole^{-1}.

Focusing on the more reliable RCCSD(T) results of the $\tilde{X}\,^1A_1$ state of SbO_2^-, the computed equilibrium bond angle (θ_e) decrease from 112.41° to 111.19° (Table IV) as the basis size/quality is improved from basis sets B to E. Based on this computed trend, it is concluded that the equilibrium bond angle of 111.19° obtained with the largest basis set E is probably an upper limit of the true value. Based on the range of

TABLE IV. The optimized geometrical parameters (r_e in Å and θ_e in deg), computed harmonic vibrational frequencies (ω_e's in cm^{-1}), and relative electronic energies [T_e in kcal/mole (eV)] of low-lying singlet and triplet electronic states of SbO_2^- obtained at different levels of calculation (for basis sets used, see Table I).

SbO_2^-	States	r_e	θ_e	ω_e (a_1,a_1,b_2)[a]	T_e
B3LYP/A	$^3B_1$	1.9179	119.21	637.1,188.1,498.4	40.9(1.776)
	$^1A_1$	1.8690	111.70	767.2,255.4,759.6	0.0
HCTH407/A	$^3B_1$	1.9216	121.56	616.1,187.6,578.0	40.7(1.763)
	$^1A_1$	1.8764	112.00	731.2,242.8,724.0	0.0
PW91PW91/A	$^3B_1$	1.9282	121.10	620.8,184.4,587.8	41.2(1.785)
	$^1A_1$	1.8862	111.76	725.7,236.0,719.2	0.0
MP2/A	$^3B_1$	1.8642	134.29	806.3,210.7,2667.3	55.4(2.402)
	$^1A_1$	1.8748	112.16	759.0,248.4,763.6	0.0
CASSCF/B1	$^3A_1$	2.0078	107.90		86.8(3.762)
	$^3A_2$	1.9409	90.20		52.4(2.271)
	$^3B_1$	1.9208	116.15		50.9(2.209)
	$^3B_2$	1.9636	100.11		50.0(2.169)
	$^1A_1$	1.8595	111.15	748.5,275.5,730.2	0.0
RCCSD(T)/B	$^3B_2$	1.9450	99.57		56.7(2.461)
	$^3A_2$	1.9258	89.70		52.0(2.253)
	$^3B_1$	1.8946	120.81	661.8,190.7,750.6	48.8(2.115)
	$^1A_1$	1.8568	112.41	764.6,263.9,764.5	0.0
CASSCF/MRCI/B	$^1A_1$	1.8569[b]	112.16[b]	(762.5,267.4)[c] [758.2,266.9][d]	
RCCSD(T)/C	$^3B_2$	1.9648	99.29		56.9(2.467)
	$^3A_2$	1.9422	84.97		51.3(2.223)
	$^3B_1$	1.9100	121.05	664.4,173.4,772.1	48.1(2.087)
	$^1A_1$	1.8723	111.81	774.7,246.3,775.5	0.0
RCCSD(T)/D	$^1A_1$	1.8488	111.29		
RCCSD(T)/E	$^1A_1$	1.8482	111.19		

[a]Symmetric stretching, bending, and asymmetric stretching modes.
[b]From potential energy functions; this work.
[c]Computed harmonic vibrational frequencies of the symmetric stretching and bending modes obtained from the CASSCF/MRCI/B potential energy function; see text.
[d]Computed fundamental vibrational frequencies of the symmetric stretching and bending modes obtained from the CASSCF/MRCI/B potential energy function; see text.

the computed θ_e values obtained using different basis sets, the largest theoretical uncertainty associated with this upper limit is estimated to be less than 1°. Regarding computed equilibrium bond lengths (r_e) of the $\tilde{X}\,^1A_1$ state of SbO_2^- obtained at the RCCSD(T) level with different basis sets, the values increase from 1.8568 A with basis set B to 1.8723 Å with basis set C (Table IV). However, the computed values of r_e decrease to 1.8488 and 1.8482 Å with basis sets D and E, respectively. Based on all these computed values, the best theoretical r_e value is estimated to be 1.85 ± 0.01 Å. The effects of basis set extension, as shown from the results obtained employing basis sets of quadruple (basis set B) and of quintuple zeta (basis set C) quality, and the effects of the inclusion of outer core correlation (of Sb) using basis sets D and E, on the computed values of r_e and θ_e, are different. Nevertheless, it appears that the effects of correlation arising from the inclusion of $4s^24p^6$ core electrons of Sb on the computed minimum-energy geometrical parameters are insignificantly small (of the order of 0.0006 Å and 0.1°, differences between using basis sets D and E) and can therefore be ignored.

Harmonic vibrational frequencies have been computed employing basis sets B and C at the RCCSD(T) level for both the $\tilde{X}\,^1A_1$ and $\tilde{a}\,^3B_1$ states of SbO_2^- (Table IV). For each state, the differences between the computed values using these two basis sets are less than 20 cm^{-1}, which may be taken as the estimated theoretical uncertainty of these values. Fundamental and harmonic vibrational frequencies of the symmetric stretching and bending modes have been calculated using the CASSCF/MRCI/B PEF for the $\tilde{X}\,^1A_1$ state. The differences between the computed fundamental and harmonic vibrational frequencies are small (<5 cm^{-1}), suggesting small anharmonicities for both the symmetric stretching and bending modes at least near the equilibrium geometry. Computed harmonic vibrational frequencies of these two symmetric vibrational modes were obtained from both the

TABLE V. The optimized geometrical parameters (r_e in Å and θ_e in deg), computed harmonic vibrational frequencies (ω_e's in cm^{-1}), and relative electronic energies [T_e in kcal/mole (eV)] of some low-lying doublet states of SbO_2 obtained at different levels of calculation (for basis sets used, see Table I).

Method	States	r_e	θ_e	ω_e (a_1, a_1, b_2)[a]	T_e
RCCSD(T)/B[b]	$\tilde{B}\,^2A_2$	1.8905	100.96		10.7(0.463)
CASSCF/MRCI/B		1.8925[c]	101.07[c]	(720.1, 247.3)[d] [715.9, 246.9][e]	
RCCSD(T)/B[b]	$\tilde{A}\,^2B_2$	1.8686	89.13		5.0(0.217)
CASSCF/MRCI/B		1.8732[c]	89.80[c]	(752.6, 223.4)[d]; [748.2, 224.2][e]	
RCCSD(T)/B[b]	$\tilde{X}\,^2A_1$	1.8363	122.81	762.4, 205.1, 829.0	0.0
CASSCF/MRCI/B		1.8406[c]	121.76[c]	(747.1, 204.8)[d]; [742.9, 204.6][e]	
RCCSD(T)/C[b]	$\tilde{B}\,^2A_2$	1.9077	100.35		10.6(0.460)
	$\tilde{A}\,^2B_2$	1.8843	88.09		4.71(0.204)
	$\tilde{X}\,^2A_1$	1.8514	122.88		0.0
RCCSD(T)/D[b]	$\tilde{B}\,^2A_2$	1.8820	100.31		10.7(0.463)
	$\tilde{A}\,^2B_2$	1.8597	87.94		4.5(0.195)
	$\tilde{X}\,^2A_1$	1.8277	121.87		0.0
RCCSD(T)/E	$\tilde{B}\,^2A_2$	1.8812	100.26		10.6(0.462)
	$\tilde{A}\,^2B_2$	1.8590	87.84		4.4(0.190)
	$\tilde{X}\,^2A_1$	1.8277[b]	121.87[b]		0.0

[a]Symmetric stretching, bending, and asymmetric stretching modes.
[b]These geometry optimization calculations were carried out in our previous study (Ref. 6).
[c]From potential energy functions; this work.
[d]Computed harmonic vibrational frequencies of the symmetric stretching and bending modes obtained from the CASSCF/MRCI/B potential energy function; see text.
[e]Computed fundamental vibrational frequencies of the symmetric stretching and bending modes obtained from the CASSCF/MRCI/B potential energy function; see text.

CASSCF/MRCI/B PEF and numerical second derivative calculations at the RCCSD(T)/B level, and their values agree to within 4 cm^{-1}, suggesting that the electronic energy surfaces obtained from CASSCF/MRCI and RCCSD(T) calculations are similar at least in the region near the equilibrium geometry.

Results from additional calculations on some low-lying states of SbO_2 obtained in the present study and also some relevant results from our previous work[6] are summarized in Table V. Similar to results obtained for SbO_2^- discussed above, computed values of r_e for all three lowest-lying states of SbO_2 increase from using basis set B to basis set C but then decrease from using basis set C to basis sets D and E. The estimated uncertainties associated with the computed r_e values are of the order of ±0.01 Å. For computed values of θ_e, the trends for the $\tilde{A}\,^2B_2$ and $\tilde{B}\,^2A_2$ states of SbO_2 are the same as above for the $\tilde{X}\,^1A_1$ state of SbO_2^-, where the computed θ_e values decrease from using basis sets B to E. It is therefore concluded that the computed θ_e values obtained with the largest basis set E are upper limits of the true values for these two states of SbO_2. However, for the $\tilde{X}\,^2A_1$ state of SbO_2, the computed θ_e values behave like the computed r_e values, which increase and then decrease with basis set improvement. Nevertheless, the ranges of the computed θ_e values for all three states of SbO_2 considered are less than 1.3°. The estimated maximum uncertainties associated with the computed θ_e values reported in the present study for the three lowest-lying states of SbO_2 should be less than 1°.

Harmonic and fundamental vibrational frequencies of the symmetric stretching and bending modes for the $\tilde{X}\,^2A_1$, $\tilde{A}\,^2B_2$, and $\tilde{B}\,^2A_2$ states of SbO_2 obtained from CASSCF/MRCI/B PEFs are reported here for the first time (Table V). These computed harmonic and fundamental vibrational frequencies are close to each other, suggesting that anharmonic effects are small near the equilibrium geometries of these electronic states. For the $\tilde{X}\,^2A_1$ state, harmonic vibrational frequencies have been obtained previously at the RCCSD(T)/B level by numerical derivative calculations.[6] The agreement in the computed bending frequencies between the CASSCF/MRCI/B and RCCSD(T)/B values is excellent. The difference between the RCCSD(T)/B and CASSCF/MRCI/B values of the computed harmonic stretching frequency is 15 cm^{-1}.

Computed EAs and VDEs of the first three photodetachment bands (in eV) to the $\tilde{X}\,^2A_1$, $\tilde{A}\,^2B_2$, and $\tilde{B}\,^2A_2$ states of SbO_2 from the $\tilde{X}\,^1A_1$ state of SbO_2^- obtained at different levels of calculation are summarized in Table VI. Firstly, the

TABLE VI. Computed electron affinities (EAs) and vertical electron detachment energies (VDEs) of the first three photodetachment bands (in eV) to the $\tilde{X}\,^2A_1$, $\tilde{A}\,^2B_2$, and $\tilde{B}\,^2A_2$ states of SbO_2 from the $\tilde{X}\,^1A_1$ state of SbO_2^-, obtained at different levels of calculations.

	$\tilde{X}\,^2A_1$		$\tilde{A}\,^2B_2$		$\tilde{B}\,^2A_2$	
Methods	EA	VDE	EA	VDE	EA	VDE
RCCSD/B	3.626	3.717	3.819	4.157	4.002	4.128
RCCSD(T)/B	3.542	3.613	3.759	4.102	4.005	4.149
RCCSD/B2//RCCSD(T)/B		3.720		4.159		4.129
RCCSD(T)/B2//RCCSD(T)/B		3.616		4.106		4.152
RCCSD/C	3.642	3.739	3.822	4.167	4.026	4.148
RCCSD(T)/C	3.560	3.635	3.764	4.107	4.020	4.165
RCCSD/D	3.646	3.746	3.817	4.164	4.047	4.161
RCCSD(T)/D	3.562	3.637	3.757	4.102	4.025	4.160
SO contributions (all e's)[a] cm^{-1}		−2.9		+0.6		+2.3
SO contributions (ECP48MDF)[b] cm^{-1}		−2.2		−11.0		+13.1
RCCSD/E//RCCSD(T)/D	3.647	3.745	3.811	4.161	4.046	4.159
RCCSD(T)/E//RCCSD(T)/D	3.561	3.635	3.752	4.098	4.023	4.147
RCCSD/E	3.647		3.811		4.045	
RCCSD(T)/E	3.561		3.752		4.023	
CAS/B//RCCSD(T)/B		2.007		2.415		2.337
CAS/MRCI/B//RCCSD(T)/B		3.048		3.490		3.521
CAS/MRCI+D/B//RCCSD(T)/B		3.498		3.945		4.019
CAS/C//RCCSD(T)/C		2.018		2.387		2.306
CAS/MRCI/C//RCCSD(T)/C		3.071		3.487		3.518
CAS/MRCI+D/C//RCCSD(T)/C		3.354		3.770		3.853

[a]Contributions from CASSCF spin-orbit (SO) interaction calculations between the $\tilde{X}\,^2A_1$, $\tilde{A}\,^2B_2$, and $\tilde{B}\,^2A_2$ states of SbO_2, using uncontracted s, p, and d functions of the DZVP-DFT-orb basis sets for Sb and O, and the RCCSD(T)/D electronic energies of these three states for the diagonal SO matrix elements. The CASSCF SO calculations were carried out at the RCCSD(T)/D geometry of the $\tilde{X}\,^1A_1$ state of SbO_2^- (also see text).
[b]As footnote a, except that the spin-orbit effective core potential, ECP48MDF was used for Sb and the uncontracted s, p, and d functions of the ECP48MWB_aug-cc-pVQZ and aug-cc-pVQZ basis sets were used for Sb and O, respectively (also see text).

CASSCF level is clearly inadequate for relative electronic energies. In addition, both contributions from triple excitations of the RCCSD(T) calculations and the Davidson corrections of the MRCI calculations to the computed EA and/or VDE values are significant, with the latter contributions being more significant. These results show that higher order dynamic electron correlation is important for calculating reliable EAs of SbO_2 and VDEs of SbO_2^-. Secondly, the computed VDE values of SbO_2^- obtained at the MRCI+D level are consistently smaller than those obtained at the RCCSD(T) level with the same basis sets. Nevertheless, contributions from triple excitations in the RCCSD(T) calculations and from the Davidson corrections in the MRCI calculations bring the computed RCCSD(T) and MRCI+D VDE values closer to each other compared with the corresponding RCCSD and MRCI values. Thirdly, basis set extension and core correlation effects on computed EA and VDE values are negligibly small (of the order of 0.02 eV) with the RCCSD(T) method. However, basis set extension effects on computed VDE values are considerably larger with the MRCI method (up to 0.15 eV; Table VI). From a theoretical viewpoint, the RCCSD(T) method is superior to the MRCI method because the former is size consistent, but the latter is not. From a computational viewpoint, the RCCSD(T) method is considerably less demanding than the MRCI method with the same basis set. With the MRCI method, basis set C is the largest basis set which could be used within the computational capacity available in this work. (For the low-lying doublet electronic states of SbO_2 considered, the total number of internally contracted and of uncontracted configurations are 19.5×10^6 and over 9×10^9, respectively, when basis set C is used.) Fourthly, zero-point vibrational energy (ZPVE) corrections to computed EAs for all three photodetachment bands considered, as estimated from the computed vibrational frequencies obtained in the present study, are negligibly small (less than 0.005 eV, when the fundamental frequencies of the two symmetric vibrational modes are used to evaluate ZPVE). In conclusion, based on the RCCSD(T) results obtained using different basis sets in this work, the computed EA and VDE values obtained at the highest level of calculation [i.e., the RCCSD(T)/E level] should be accurate to ±0.01 eV [estimated based on the largest differences between the corresponding computed RCCSD(T)/E and RCCSD(T)/B values of less than 0.02 eV]. However, the VDE position of a photodetachment band depends on FC factors between the two electronic states involved, which will be discussed in the next section.

Before proceeding to the next section, it should be noted that VDEs were also computed employing basis sets of double-augmented quality (basis set B2; see Table I) and the differences between the computed VDE values using basis sets B and B2 are negligibly small. These calculations em-

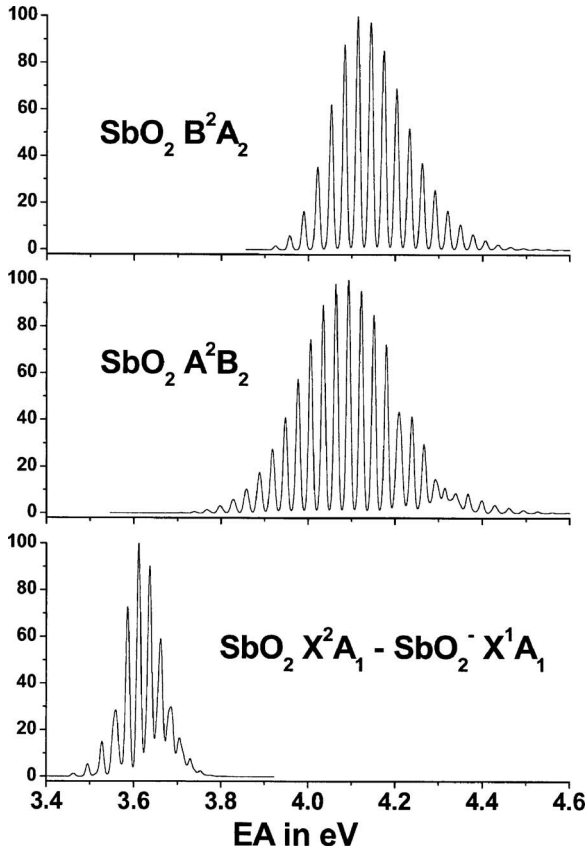

FIG. 1. The photodetachment spectrum of SbO_2^- in the 3.4–4.6 eV electron affinity (EA in eV) region simulated with Gaussian vibrational bands with full width at half maximum (FWHM) of 0.01 eV. The $\tilde{X}\,^2A_1(SbO_2) \leftarrow \tilde{X}\,^1A_1(SbO_2^-)$ band (bottom), $\tilde{A}\,^2B_2(SbO_2) \leftarrow \tilde{X}\,^1A_1(SbO_2^-)$ band (middle), and $\tilde{B}\,^2A_2(SbO_2) \leftarrow \tilde{X}\,^1A_1(SbO_2^-)$ band (top); for the relative intensity of the *y* axis, the vibrational component with the maximum intensity is set to 100 arbitrary units (the same for other figures; see text).

ploying basis set B2, which include an extra set of diffuse functions, were for the purpose of making sure that the $\tilde{X}\,^1A_1$ state of SbO_2^- obtained in this work is not an electronic state with a dipole-bound electron in a diffuse orbital. In fact, the computed Hartree-Fock and CASSCF wave functions of all the anionic states of SbO_2^- obtained in the present study show that they are valence states with all occupied molecular orbitals having negligibly small contributions from diffuse functions (see Ref. 23).

PEFs, anharmonic vibrational wave functions, and simulated photodetachment spectrum

The fitted CASSCF/MRCI/B PEFs [see Eqs. (1)–(3)] of the $\tilde{X}\,^1A_1$ state of SbO_2^- and the $\tilde{X}\,^2A_1$, $\tilde{A}\,^2B_2$, and $\tilde{B}\,^2A_2$ states of SbO_2 and the root-mean-square deviations of the fitted PEFs from the *ab initio* energy points are placed in the EPAPS supplementary material.[24] The first three photodetachment bands to the $\tilde{X}\,^2A_1$, $\tilde{A}\,^2B_2$, and $\tilde{B}\,^2A_2$ states of SbO_2, which are in the 3.4–4.6 eV EA region, have been simulated with a Gaussian linewidth of 0.01 eV full width at half maximum (FWHM) for each vibrational component and are shown in Fig. 1. In the FC factor calculations and spectral simulations, the CASSCF/MRCI/B PEFs and the EAs and optimized geometries of the states involved obtained at the highest level, the RCCSD(T)/E level, of calculation were used. From Fig. 1, it can be seen that the first three photodetachment bands of SbO_2^- are in the 3.4–3.8, 3.6–4.6, and 3.9–4.6 eV EA regions, respectively. The first band is expected to be separated from the second band, but the second and third bands will overlap heavily with each other. More detailed vibrational structures of these three photodetachment bands are shown separately in Figs. 2, 3, and 4 (placed in EPAPS supplementary material),[24] where a FWHM of 0.001 eV was used in the simulations in order to show the vibrational structure more clearly. The computed FC factors of some major vibrational progressions and their vibrational designations are also given in these figures.

For the $\tilde{X}\,^2A_1(SbO_2) \leftarrow \tilde{X}\,^1A_1(SbO_2^-)$ photodetachment band the major vibrational progression is the $(0,v_2',0) \leftarrow (0,0,0)$ progression. This is expected, as the change in the equilibrium bond angle of 10.68° [at the RCCSD(T)/E level; see Tables IV and V] upon photodetachment is quite large. The vibrational component in this progression, which has the largest computed FC factor, is the $(0,2,0) \leftarrow (0,0,0)$ transition and it gives the VDE position of 3.612 eV for this photodetachment band. The first observable vibrational component at 3.462 eV EA is actually a "hot" band arising from the $(0,0,0) \leftarrow (0,3,0)$ transition. The $(0,0,0) \leftarrow (0,0,0)$ component at 3.561 eV EA, which gives the adiabatic EA, has a significant computed FC factor but is very close in energy to the hot band component, $(0,1,0) \leftarrow (0,1,0)$ at 3.553 eV EA. With a typical photodetachment experimental resolution (e.g., 30 meV), these two vibrational components are not expected to be resolvable [see, for example, the simulated first photodetachment band with a FWHM of 0.01 eV in Fig. 1 (bottom trace)]. Lastly, with a Boltzmann vibrational temperature of 300 K, hot bands arising from the (0,1,0), (0,2,0), (1,0,0), and (0,3,0) vibrational levels of the $\tilde{X}\,^1A_1$ state of SbO_2^- should be observable in all three simulated photodetachment bands.

The major vibrational progression of the simulated $\tilde{A}\,^2B_2(SbO_2) \leftarrow \tilde{X}\,^1A_1(SbO_2^-)$ photodetachment band is the $(0,v_2',0) \leftarrow (0,0,0)$ progression. However, the $(0,0,0) \leftarrow (0,0,0)$ vibrational component at 3.752 eV has a very small computed FC factor and hence is not observable in the simulated spectrum. This is because the change in the equilibrium bond angle upon photodetachment is 20.35° [at the RCCSD(T)/E level], which is very large. The first observable vibrational component of this photodetachment band is probably due to the hot band transition, $(0,4,0) \leftarrow (0,3,0)$ or $(0,5,0) \leftarrow (0,3,0)$ at 3.765 or 3.793 eV EA, respectively. As for the main vibrational progression, $(0,v_2',0) \leftarrow (0,0,0)$, it is the 13th component (i.e., $v_2'=12$) which has the largest computed FC factor. It should be noted that the computed anharmonic vibrational wave functions of the $\tilde{A}\,^2B_2$ state of SbO_2 indicate that there is considerable mixing between $(0,v_2',0)$ levels, with $v_2'=16$, 17, and 18, and $(1,v_2',0)$ levels, with $v_2'=11$, 12, and 13, respectively. It should also be noted that the assignments of the v_2' quantum numbers of these few vibrational levels are only tentative, as the largest computed coefficients of the harmonic basis functions in the anhar-

monic vibrational wave functions are only of the order of 0.3, suggesting very strong mixing. From the computed irregular relative vibrational energy separations of these few anharmonic vibrational levels, the interactions of these few vibrational levels are almost certainly due to Fermi resonances. Consequently, these interactions lead to irregular computed FC factors and energy positions for transitions to these upper state vibrational levels in the 4.2 eV EA region of the simulated photodetachment spectrum (see the bar diagrams of the FC factors of some major vibrational progressions given in Fig. 3, which is placed in the EPAPS supplementary material[24]).

The main vibrational progression in the simulated $\tilde{B}\,^2A_2(SbO_2) \leftarrow \tilde{X}\,^1A_1(SbO_2^-)$ photodetachment band is again the $(0,v_2',0) \leftarrow (0,0,0)$ progression. The vibrational component with the strongest computed FC factor in this progression is the $(0,2,0) \leftarrow (0,0,0)$ component at 4.084 eV EA. The first observable vibrational component is the hot band, $(0,0,0) \leftarrow (0,3,0)$ component, at 3.924 eV EA. The $(1,v_2',0) \leftarrow (0,0,0)$ progression and, to a lesser extent, the $(2,v_2',0) \leftarrow (0,0,0)$ progression are computed to have significant intensities. This is because, in addition to the change in the equilibrium bond angle of 10.93° upon photodetachment, the change in the equilibrium bond length of 0.033 Å is the largest of the three photodetachment processes considered.

Lastly, a mistake in our previous studies[5,6] regarding SO interaction calculations that were carried out employing a spin-orbit pseudopotential has to be corrected. The reported ECP46MWB ECP used in our previous studies for SO calculations should actually be the ECP46MDF ECP used in the present study, as a SO pseudopotential is available for the latter ECP, but not the former. Nevertheless, the conclusion made in our previous studies[5,6] that contributions from off-diagonal SO interaction to computed relative electronic energies are negligibly small is still valid with the ECP46MDF ECP. For the sake of completeness, computed relative electronic energies, without and with SO contributions (calculated employing the ECP46MDF ECP), of eight low-lying doublet states and four low-lying quartet states of SbO_2 are given in Table VII. The lowering in energy of the $\tilde{X}\,^2A_1$ state of SbO_2 by SO interaction is $-31.8\ cm^{-1}$. The T_e values of the $\tilde{A}\,^2B_2$ and $\tilde{B}\,^2A_2$ states of SbO_2 are decreased and increased by SO contributions by -1.3 and $+14.8\ cm^{-1}$, respectively. The $\tilde{X}\,^1A_1$ state of SbO_2^+ is lowered by $-0.5\ cm^{-1}$ by SO contributions and the vertical ionization energies to the $\tilde{a}\,^3B_2$ and $\tilde{b}\,^3A_2$ states of SbO_2^+ are both increased by $+0.07\ cm^{-1}$ by SO contributions using a SO pseudopotential. Summing up, off-diagonal SO contributions to computed relative electronic energies are negligibly small for low-lying electronic states of SbO_2 and its ions.

TABLE VII. Computed relative electronic energies [T_v, vertical excitation energies in kcal/mole (eV)] of low-lying doublet and quartet states of SbO_2 without [computed using the CASSCF/MRCI+D method with basis set B at the CASSCF/MRCI+D/B optimized geometry of the $\tilde{X}\,^2A_1$ state of SbO_2 (from Ref. 6)] and with (T_v+SO) spin-orbit (SO) interaction [using the B_SO basis set (see Table I) and the SO pseudopotential ECP46MDF ECP; see text].

States	T_v	T_v+SO
$\tilde{X}\,^2A_1$	0	0
(1) $^2B_2$	19.0 (0.82)	18.7 (0.81)
(1) $^2A_2$	19.6 (0.85)	20.2 (0.88)
(1) $^2B_1$	51.2 (2.22)	50.2 (2.18)
(2) $^2A_1$	53.1 (2.30)	53.6 (2.32)
(2) $^2B_2$	59.7 (2.59)	60.4 (2.62)
(2) $^2B_1$	67.7 (2.93)	67.8 (2.94)
$^4B_2$	70.1 (3.04)	70.3, 70.5 (3.05, 3.06)
$^4A_2$	70.7 (3.07)	71.1, 71.2 (3.08, 3.09)
(2) $^2A_2$	81.0 (3.51)	81.1 (3.52)
$^4A_1$	87.4 (3.79)	87.7, 87.8 (3.80, 3.81)
$^4B_1$	98.7 (4.28)	99.1, 99.2 (4.30, 4.30)

CONCLUDING REMARKS

State-of-the-art *ab initio* calculations have been carried out on low-lying electronic states of SbO_2^-. The ground electronic state of SbO_2^- is found to be the $\tilde{X}\,^1A_1$ state and the lowest excited state is the $\tilde{a}\,^3B_1$ state, calculated to be ~48 kcal $mole^{-1}$ (2.1 eV) higher in energy. Further higher level calculations than previously performed have also been carried out on the $\tilde{X}\,^2A_1$, $\tilde{A}\,^2B_2$, and $\tilde{B}\,^2A_2$ states of SbO_2. Potential energy functions of the $\tilde{X}\,^1A_1$ state of SbO_2^- and the $\tilde{X}\,^2A_1$, $\tilde{A}\,^2B_2$, and $\tilde{B}\,^2A_2$ states of SbO_2 have been computed at the CASSCF/MRCI level in order to simulate the photodetachment spectrum of SbO_2^- in the EA region of 0–4.6 eV. While the first photodetachment band to the $\tilde{X}\,^2A_1$ state of SbO_2 is largely separated from the second and third photodetachment bands to the $\tilde{A}\,^2B_2$ and $\tilde{B}\,^2A_2$ states of SbO_2, the latter two bands overlap significantly. For each of these three photodetachment bands, the vibrational structure involves a long vibrational progression in the bending mode of the upper state, particularly for the second band involving photodetachment to the $\tilde{A}\,^2B_2$ state of SbO_2. The present study has completed a study on SbO_2 and its ions with the main aim of providing information to assist their future spectral identification.

Lastly, it should be noted that possible nonadiabatic interactions between low-lying electronic states of SbO_2 and Darling-Dennison interactions between $2\nu_1$ and $2\nu_3$ of each electronic state of SbO_2/SbO_2^- have not been considered in the present study. Since the energy separations between low-lying electronic states of SbO_2 and the energy difference between ν_1 and ν_3 of each electronic state of SbO_2/SbO_2^- studied are quite small, both nonadiabatic and Darling-Dennison interactions could be significant. These interactions would cause the observed photodetachment spectrum of SbO_2^- to be more complex than the simulated one reported here. Nevertheless, the present study should provide a basis for further investigations on these more subtle effects (see, for example, Refs. 25 and 26), though it is unlikely that a typical moderate-resolution laser photodetachment experiment (such as that of Ref. 21 or 22) would yield a spectrum, which would reveal such effects.

ACKNOWLEDGMENTS

The authors are grateful to the Research Grant Council (RGC) of the Hong Kong Special Administrative Region (HKSAR, Grant No. PolyU 5014/06) and the Research Committee of the Hong Kong Polytechnic University of HKSAR (Grant Nos. G-YE06 and G-YG09) for financial support. The provision of computational resources from the EPSRC (UK) National Service for Computational Chemistry Software is also acknowledged. EPFL is grateful to Professor Hermann Stoll (Stuttgart) for very helpful advice in the use of spin-orbit pseudopotentials in spin-orbit interaction calculations.

[1] Y. W. Wang, B. H. Hong, J. Y. Lee, J.-S. Kim, G. H. Kim, and K. S. Kim, J. Phys. Chem. B **108**, 16723 (2004).
[2] Y. W. Wang, J. S. Kim, G. H. Kim, and K. S. Kim, Appl. Phys. Lett. **88**, 143106 (2006).
[3] S. H. Taylor, J. S. J. Hargreaves, G. J. Hutchings, and R. W. Joyner, Appl. Catal., A **126**, 287 (1995).
[4] G. Centi and S. Perathoner, Appl. Catal., A **124**, 317 (1995).
[5] E. P. F. Lee, J. M. Dyke, F.-T. Chau, W.-K. Chow, and D. K. W. Mok, Chem. Phys. Lett. **429**, 365 (2006).
[6] E. P. F. Lee, J. M. Dyke, F.-T. Chau, W.-K. Chow, and D. K. W. Mok, J. Chem. Phys. **125**, 064307 (2006).
[7] C. Xu, E. de Beer, and D. M. Neumark, J. Chem. Phys. **104**, 2749 (1996).
[8] M. L. Martin and J. Sundermann, J. Chem. Phys. **114**, 3408 (2001).
[9] K. A. Peterson, J. Chem. Phys. **119**, 11099 (2003); see also http://www.theochem.uni-stuttgart.de/cgi-bin/pe.sh?References
[10] http://www.emsl.pnl.gov/forms/basisform.html The Extensible Computational Chemistry Environment Basis Set Database, Version 02/25/04, as developed and distributed by the Molecular Science Computing Facility, Environmental and Molecular Sciences Laboratory which is part of the Pacific Northwest Laboratory, P.O. Box 999, Richland, Washington 99352, USA, and funded by the U.S. Department of Energy. The Pacific Northwest Laboratory is a multiprogram laboratory operated by Battelle Memorial Institute for the U.S. Department of Energy under Contract No. DE-AC06-76RLO 1830. Contact Karen Schuchardt for further information.
[11] N. Godbout, D. R. Salahub, J. Andzelm, and E. Wimmer, Can. J. Chem. **70**, 560 (1992).
[12] H. Stoll, B. Metz, and M. Dolg, J. Comput. Chem. **23**, 767 (2002).
[13] H.-J. Werner, P. J. Knowles, M. Schütz *et al.*, MOLPRO is a package of *ab initio* programs.
[14] W. Meyer, P. Botschwina, and P. Burton, J. Chem. Phys. **84**, 891 (1986).
[15] S. Carter and N. C. Handy, J. Chem. Phys. **87**, 4294 (1987).
[16] J. E. Dennis, Jr., D. M. Gay, and R. E. Welsh, ACM Trans. Math. Softw. **7**, 348 (1981); **7**, 369 (1981).
[17] J. K. G. Watson, Mol. Phys. **15**, 479 (1968).
[18] D. W. K. Mok, E. P. F. Lee, F.-T. Chau, D.-C. Wang, and J. M. Dyke, J. Chem. Phys. **113**, 5791 (2000).
[19] J. M. Dyke, E. P. F. Lee, D. K. W. Mok, and F.-T. Chau, ChemPhysChem **6**, 2046 (2005).
[20] F.-T. Chau, J. M. Dyke, E. P. F. Lee, and D. K. W. Mok, J. Chem. Phys. **115**, 5816 (2001).
[21] H. Wu and L.-S. Wang, J. Phys. Chem. A **102**, 9129 (1998).
[22] G. L. Gutsev, P. Jena, H.-J. Zhai, and L.-S. Wang, J. Chem. Phys. **115**, 7935 (2001).
[23] E. P. F. Lee, J. Lozille, P. Soldan, and T. G. Wright, Chem. Phys. Lett. **336**, 479 (2001).
[24] See EPAPS Document No. E-JCPSA6-127-302732 for the potential energy functions (PEFs) of the $\tilde{X}\,^1A_1$ state of SbO_2^- and the $\tilde{X}\,^2A_1$, $\tilde{A}\,^2B_2$, and $\tilde{B}\,^2A_2$ states of SbO_2 and the simulated $\tilde{X}\,^2A_1(SbO_2) \leftarrow \tilde{X}\,^1A_1(SbO_2^-)$, $\tilde{A}\,^2B_2(SbO_2) \leftarrow \tilde{X}\,^1A_1(SbO_2^-)$, and $\tilde{B}\,^2A_2(SbO_2) \leftarrow \tilde{X}\,^1A_1(SbO_2^-)$ photodetachment bands (Figs. 2, 3, and 4, respectively) with a FWHM of 0.001 eV (the computed Franck-Condon factors of some major vibrational series and their designations are also given). This document can be reached through a direct link in the online article's HTML reference section or via the EPAPS homepage (http://www.aip.org/pubservs/epaps.html).
[25] S. Mahapatra, H. Koppel, L. S. Cederbaum, P. Stampfub, and W. Wenzel, Chem. Phys. **259**, 211 (2000).
[26] Y. Morino and M. Tanimoto, J. Mol. Spectrosc. **166**, 310 (1994).